Synthesis and Structural Evolution of Nickel–Cobalt Nanoparticles Under H_2 and CO_2

*Sophie Carenco, Cheng-Hao Wu, Andrey Shavorskiy, Selim Alayoglu, Gabor A. Somorjai, Hendrik Bluhm, and Miquel Salmeron**

Bimetallic nanoparticle (NP) catalysts are interesting for the development of selective catalysts in reactions such as the reduction of CO_2 by H_2 to form hydrocarbons. Here the synthesis of Ni–Co NPs is studied, and the morphological and structural changes resulting from their activation (via oxidation/reduction cycles), and from their operation under reaction conditions, are presented. Using ambient-pressure X-ray photoelectron spectroscopy, X-ray absorption spectroscopy, and transmission electron microscopy, it is found that the initial core–shell structure evolves to form a surface alloy due to nickel migration from the core. Interestingly, the core consists of a Ni-rich single crystal and a void with sharp interfaces. Residual phosphorous species, coming from the ligands used for synthesis, are found initially concentrated in the NP core, which later diffuse to the surface.

1. Introduction

While the historical level of 400 ppm of atmospheric CO_2 was reached in May 2013, research on catalytic chemical,[1] electrochemical,[2] and photochemical[3,4] processes that use it as a feedstock has strongly increased over the last decade. Amongst these processes, the chemical reduction of CO_2 by H_2 (sometimes called CO_2-based Fischer-Tropsch Synthesis)[5] could provide clean synthetic fuels as well as a variety of chemicals such as oxygenates.[6–8] To achieve this, CO insertion reactions should be promoted over CO_2 and CO dissociation.[9–13] Bimetallic nanoparticles (NPs), including CoCu, CoPd, and CoPt on oxide supports have been used for this purpose.[14–20] On cobalt-based catalysts, using CO_2 as a feedstock instead of CO produced intermediates that led to alkane formation.[21] On the other hand, nickel catalysts produce methane as the major product.[22] Recently, Yu et al. showed that NiCo NPs produce methane-rich mixtures of alkanes.[23] These results demonstrate the interest of moving from single-metal to bimetallic NPs, as well as the high potential of NiCo NPs for selective CO_2 reduction, in particular compared with CO reduction. In addition to its environmental relevance as a feedstock, CO_2 prevents unwanted leaching of Ni species in the form of $Ni(CO)_4$.[24]

However, more than single component NP, bimetallics are subject to structural modifications as a result of exposure to reactive gases (H_2, O_2, CO, or CO_2). For example, we have shown in a previous work that core–shell CuCo NP undergo partial dealloying when exposed to CO and H_2 even in the Torr pressure regime.[18]

Dr. S. Carenco, C.-H. Wu, Dr. A. Shavorskiy, Dr. S. Alayoglu, G. A. Somorjai, H. Bluhm
Chemical Sciences Division
Lawrence Berkeley National Laboratory
Berkeley, CA 94720, USA

C.-H. Wu, M. Salmeron
Materials Sciences Division
Lawrence Berkeley National Laboratory
Berkeley, CA 94720, USA
E-mail: mbsalmeron@lbl.gov

Dr. A. Shavorskiy
Advanced Light Source
Lawrence Berkeley National Laboratory
Berkeley, CA 94720, USA

G. A. Somorjai
Department of Chemistry
University of California Berkeley
Berkeley, CA 94720, USA

M. Salmeron
Department of Materials Sciences and Engineering
University of California Berkeley
Berkeley, CA 94720, USA

DOI: 10.1002/smll.201402795

© 2015 Wiley-VCH Verlag GmbH & Co. KGaA, Weinheim

In this study, a novel synthesis for core–shell Ni-Co NPs with 20 nm nickel core was developed by a two-step colloidal method. The structural and morphological evolution of the NPs was tracked using ex situ analysis (TEM-EDS) and in situ ambient-pressure X-ray photoelectron spectroscopy (XPS) following activation (oxidation/reduction cycles to remove ligands and to reduce the metals), as well as under model reaction conditions (mixtures of CO_2 and H_2 in the Torr pressure range).

2. Results and Discussion

2.1. Synthesis of Ni-Co Core–Shell NPs

A new protocol was developed for the synthesis of core–shell Ni-Co NPs with a narrow size distribution (**Figure 1**a and Figure S1, Supporting Information). First we followed a well-established route[25] to obtain Ni NPs of 20 ± 1 nm diameter with 100% yield. This involves reduction of $Ni(acac)_2$ (acac = acetylacetonate) by oleylamine (OAm) in the presence of trioctylphosphine (TOP). The use of TOP made possible a narrow size distribution for the Ni cores. At the end of this first step, the solution contained Ni(0) NPs mostly stabilized by TOP ligands.[25] It also contained excess TOP, as well as by-products derived from oleylamine, as extensively described elsewhere.[26]

In a second step the flask containing the product was cooled to room temperature (r.t.) and without further treatment 0.5 equiv. of $Co_2(CO)_8$ were added to the colloidal solution. The solution was first heated to 120 °C in order to fully dissolve the cobalt precursor and later to 180 °C to form the core–shell Ni-Co NPs. The advantage of this sequential process is that the by-products of the first did not interfere with the second step.[26] This second step used a Co(0) precursor, thus avoiding any galvanic reaction that would release metal cations into the solution. In contrast with other synthetic routes such as the one developed by Yamauchi et al.,[27] our protocol did not require the reduction of the cobalt precursor because it was already at the zero oxidation state. Upon addition to the Ni(0) NPs solution, $Co_2(CO)_8$ dissolves and produced a bubbling of gas. This corresponds to the partial displacement of CO by TOP in the coordination sphere of Co(0), producing $[Co^{(0)}_x(CO)_y(TOP)_z]_n$ species, well-known in organometallic chemistry (Scheme S1, Supporting Information).[28] The decomposition of the resulting cobalt(0) carbonyl phosphine complexes to metallic cobalt occurred by adsorption of the complexes on the surface and desorption of the CO molecules. It was complete at 180 °C after 1 h of reaction.[29]

Our synthesis protocol favored a core–shell morphology over homogeneous nucleation of pure Co NPs by promoting a preliminary reaction of the Co precursor with the Ni surface at 120 °C. This temperature was lower than the reported homogeneous nucleation temperature of cobalt NPs in solution (≈180 °C), observed previously.[21,30,31] Moreover, even at 180 °C nucleation on the surface is favored compared to homogeneous nucleation because of the lower surface energy. It should be noted that a complementary experiment performed with a slow heating ramp from 120 to 180 °C over 1 h produced the same NPs, suggesting that the nickel surface assisted the decomposition of the cobalt carbonyls at temperatures below 180 °C.

Transmission electron microscopy (TEM) images of the core–shell Ni-Co NPs with 1:1 Ni:Co ratio (named *NiCo* NPs hereafter) are shown in Figure 1b. The NPs were found to contain a few percent of phosphorus in the core (blue dots on Figure 1 and Figure S2, Supporting Information) due to the

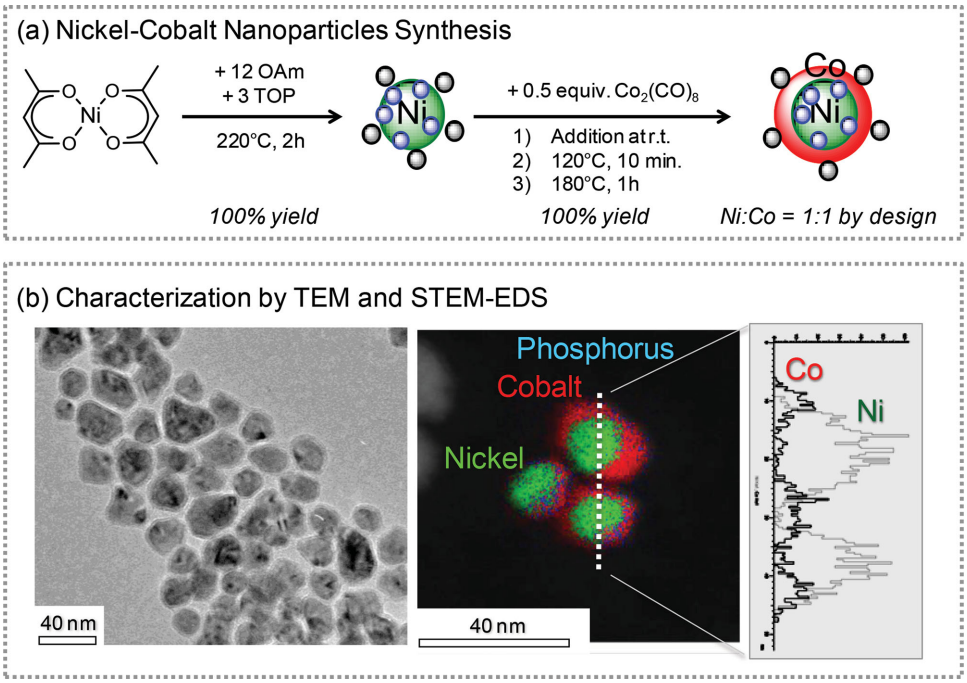

Figure 1. a) Protocol for the synthesis of core–shell Ni–Co NPs. Blue dots represent phosphide species and black dots phosphorated ligands. b) TEM-EDS characterization with color-coded map. Right: Intensity of Ni and Co EDS signal along the dotted line. Phosphorus is barely visible in the EDS.

© 2015 Wiley-VCH Verlag GmbH & Co. KGaA, Weinheim

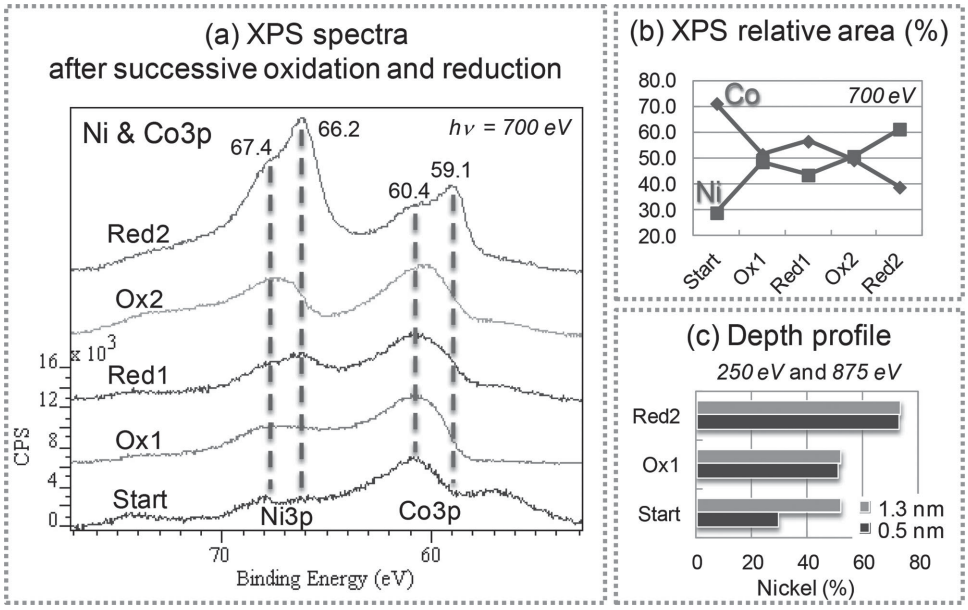

Figure 2. a) XP spectra of *NiCo* NPs after pretreatment steps (*Ox*: after oxidation, *Red*: after reduction), using a photon energy of 700 eV. b) Evolution of the relative areas of the Ni and Co peak. c) Percentage of nickel on the surface measured with electrons of 0.5 and 1.3 nm mean free path, obtained with photon energies of 250 and 875 eV, respectively.

partial decomposition of phosphorated ligands (black dots in Figure 1) in the first step, as will be discussed in Section 2.5.

The core diameter of the NPs can be tuned as shown in previous work,[25] and their overall composition adjusted by changing the amount of $Co_2(CO)_8$ injected, both steps proceeding with 100% yield. As a proof of concept, a similar reaction was conducted using 0.125 equiv. of cobalt precursor, resulting in NPs with a thin shell of Co and with overall composition of Ni:Co = 4:1 (Figure S3, Supporting Information). In this work only *NiCo* NPs with a Ni:Co = 1:1 ratio will be discussed.

The bimetallic *NiCo* NPs had a size distribution in the range of 22–40 nm with an average of 26 nm. An average composition of Ni:Co = 1:1 was measured by Energy Dispersive X-Ray Spectroscopy (EDS). At the subnanometer scale the composition showed some heterogeneity with ratios varying between 1:0.7 and 1:1.3. The local heterogeneities self-corrected later during reaction, as will be shown in Section 2.3. No pure cobalt NPs were ever observed, confirming that the Co precursor reacted exclusively with the existing Ni NPs. Larger NPs showed a Co-rich composition (Ni:Co < 1), with a few showing an asymmetric shell (Figure S1, Supporting Information). Nevertheless every NP had a shell of cobalt at least 1 nm thick, which ensured that nickel was not exposed at the start of the catalytic reaction. On the TEM images all NPs presented a lower contrast in the shell region due to oxidation of the Co near the surface upon exposure to air while transferring to the TEM.

2.2. Chemical and Structural Changes Following Oxidation and Reduction

The use of the NPs as catalysts for CO_2 reduction requires several pretreatment steps. These steps consist of cycles of oxidation under O_2 and reduction under H_2, to burn away the organic ligands and to reduce the oxides to the metallic state, respectively. It is therefore crucial to understand the effects of these steps on the NP catalyst structure.

To this end we used ambient-pressure X-ray photoelectron spectroscopy (APXPS) at beamline 11.0.2 of the Advanced Light Source in Berkeley,[32] which can operate under gas pressures ranging from high vacuum to a few Torr pressure.[33,34]

The *NiCo* NPs were dispersed in hexanes and drop-casted onto a gold foil to be analyzed by APXPS. The cleaning pretreatment consisted of two cycles of oxidation and reduction. Oxidation was performed at 1 Torr of O_2 at 220 °C for 15 min and reduction was performed at 5 Torr of H_2 at 270 °C for 15 min. After each step the sample was cooled down and spectra collected after pumping out the gases.

The Ni and Co XPS 3p region (**Figure 2**a) shows the changes in oxidation states of both metals after each cycle. The high binding energy peak of Ni3p (67.4 eV), which corresponds to the higher oxidation state, increased in intensity after oxidation (*Ox1* and *Ox2*) and decreased after reduction (*Red1* and *Red2*), while the 66.2 eV peak corresponding to reduced Ni followed the reverse trend. A similar behavior was observed for the Co3p peaks at 60.4 eV (oxide) and 59.1 eV (metallic). Partial electron yield X-ray absorption spectra (XAS) at the Co and Ni L-edges confirmed the reduced state of both metals (Figure S6, Supporting Information). It should be noted that in spite of the Ultra High Vacuum (UHV) environment the NPs underwent partial reoxidation within an hour due to reaction with residual gases, mainly CO, H_2O, at pressures in the 10^{-9} Torr range in the chamber.

Less expected was the significant change in the relative nickel and cobalt peak areas (Figure 2a) following the oxidation–reduction treatments. The area of the nickel peak grew compared to that of cobalt, as shown in the plot of the

© 2015 Wiley-VCH Verlag GmbH & Co. KGaA, Weinheim

relative areas (corrected by photoemission cross-sections)[35] in Figure 2b. Initially the surface of the NPs contained mostly cobalt (≈70%), but after the first oxidation (*Ox1*), both nickel and cobalt were observed on the surface in the same proportion as in the overall NPs (1:1). After the last reduction step the surface composition was ≈60% nickel, twice that in the initial state.

In these experiments, we used a photon energy of 700 eV, which produced photoelectrons with an average escape depth of ≈1.1 nm for Ni and Co.[36,37] A depth profile can be obtained using different photon energies (875 and 275 eV in our case), which produce 3p photoelectrons with mean free paths of ≈1.3 and 0.5 nm, respectively. The result, shown in Figure 2c, indicates that the initial Ni-Co stoichiometry was ≈30% Ni within a depth of 0.5 nm and ≈50% Ni within a 1.3 nm depth. However, after the first oxidation (*Ox1*) and in further steps, the NP surface was enriched in nickel compared with the initial state in both the 0.5–1.3 nm depth regions.

2.3. Morphological Evolution Studies

Although the XPS studies revealed structural changes where Ni segregates to the surface of the NPs, more detailed information of the morphological changes can only be obtained with high resolution imaging techniques. We thus carried out studies using ex situ TEM imaging in conjunction with EDS chemical mapping. For these experiments the *NiCo* NPs were deposited on a silicon nitride TEM grid and treated under conditions similar to those in the APXPS experiments (oxidation at 220 °C and reduction at 270 °C) but at a pressure of 1 bar. Although APXPS indicates that the reduction leaves the particles in the metallic state, exposure to air during transfer of to the TEM produced a thin surface oxide, which did not alter significantly the atomic distribution in the NPs.

The high-angle annular dark-field (HAADF) TEM images shown in **Figure 3** reveal that the NPs have a distribution of sizes and shapes, which became more uniform after subsequent oxidation steps (Figure 3a, *Start* and *Ox1*). No sintering was observed, although the mean diameter of the NPs increased slightly by about 10%–20%, consistent with the volume expansion due to oxidation. A gradient of concentration was observed by Scanning Transmission Electron Microscopy (STEM) with EDS mapping (Figure S4, Supporting Information), with a nickel-rich core and a cobalt-rich shell, indicating nickel–cobalt inter-diffusion during oxidation.

After the subsequent reduction (*Red1* state) the NPs presented an interesting and unexpected morphology consisting of a partially hollow core surrounded by a nearly spherical shell (Figure 3a,b, *Red1*). The mean diameter was still in the same range (26–30 nm) while retaining the spherical shape.

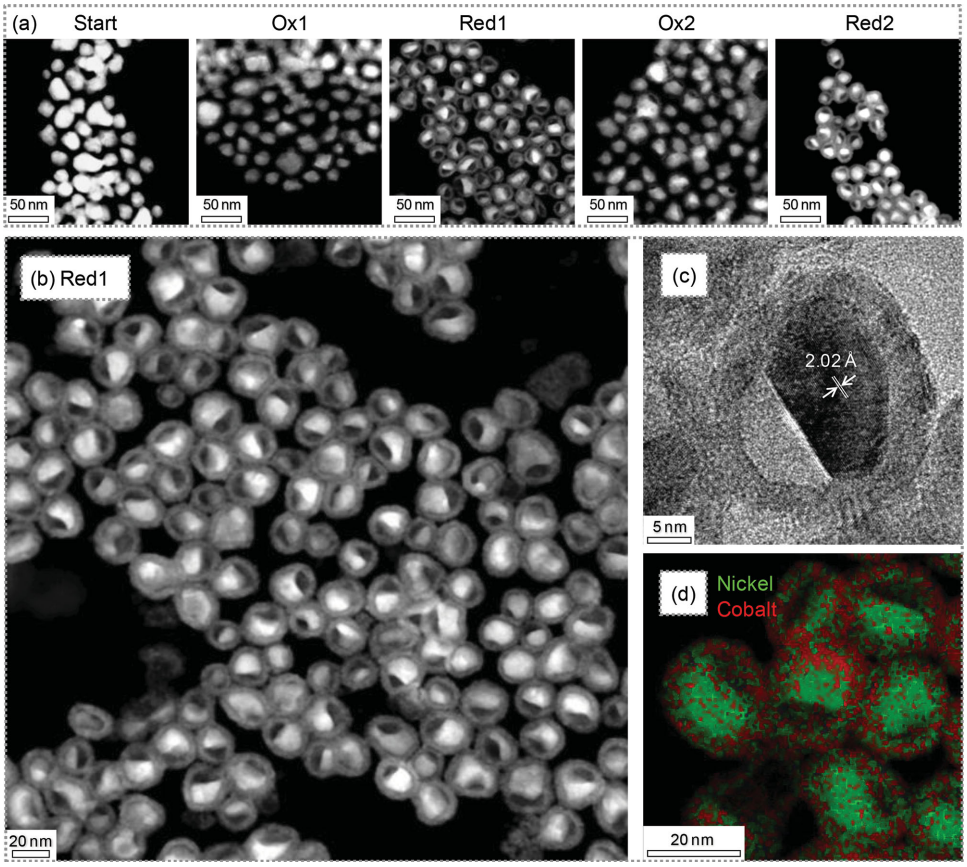

Figure 3. a) Ex situ TEM-HAADF images obtained after oxidation and reduction cycles. b) TEM-HAADF image of the *NiCo* NPs after the first oxidation–reduction cycle (*Red1* state). The NPs cores consist of a Ni rich single crystal and a void separated by sharp crystal planes. c) HRTEM image of one NP after *Red1* showing its partially filled single crystal core. The distance of 2.02 Å between lattice fringes corresponds to (111) planes of Ni or Ni-Co alloys. d) STEM-EDS nickel and cobalt maps after *Red1*.

© 2015 Wiley-VCH Verlag GmbH & Co. KGaA, Weinheim

The partially filled cores exhibited sharp interfaces that correspond to crystalline planes. As an example, Figure 3c shows a NP single-crystal core with lattice fringes separated by 2.02 Å, consistent with the (111) planes of fcc nickel or nickel–cobalt. The surrounding shell is polycrystalline. The STEM-EDS map (Figure 3d and Figure S5, Supporting Information) indicates that both the shell and the core contained nickel and cobalt, although there was a gradient of composition (Ni-rich core and Co-rich shell), reminiscent of the initial core–shell structure, as shown in the cross-cut in Figure S5, Supporting Information that confirms the presence of nickel at the surface of the NPs. This is also consistent with the APXPS data that show an increase of nickel concentration on the surface after the oxidation–reduction cycle. The EDS indicated no change in the overall NPs composition, which remained close to Ni:Co = 1:1.

A second oxidation cycle (*Ox2* state) resulted in the formation of nearly uniform NPs, although some residual voids could still be observed in the core, as shown in Figure 3a, *Ox2*. Further reduction (*Red2* state) restored the partially hollow core structure observed after the first reduction. The *Ox2* (resp. *Red2*) STEM-EDS images were similar to those from *Ox1* (resp. *Red1*) (data not shown).

In summary, the oxidation and reduction steps do not result in significant sintering of the *NiCo* NPs. The TEM study indicates that this treatment transformed the NPs from an initial inhomogeneous shape distribution to a more spherical and homogeneous one, with voids in the core occupying roughly half of the volume after reduction. The half-filled core consists mostly of single Ni-rich crystal with sharp crystal plane terminations. In addition the treatments resulted in the migration of nickel from the core to the shell, consistent with the APXPS observations.

We propose the following model to explain this morphological evolution (**Scheme 1**). During the first oxidation, a mixed nickel–cobalt oxide is formed with a consequent increase in volume (Scheme 1, *Ox1*). Upon reduction the nickel-rich region of the NP (i.e., the core) reduces faster than the shell because typical reduction temperatures are lower for nickel than for cobalt.[38,39] The reduction of the oxide in the core, due to diffusion of H to the interior and of water to the exterior, shrinks its volume and produces the void. Further heating in H_2 finally reduced the shell, producing the structure observed by TEM.

The formation of voids upon reduction does not prevent nickel–cobalt interdiffusion, as observed by XPS. One should also note that this is distinct from the nanoscale Kirkendall effect that typically results in hole formation during the oxidation step.[40] As anticipated from our proposed mechanism, the second oxidation following the first reduction step led to expansion of the core, which filled most of the void region (*Ox2*), while the second reduction (*Red2*) recreated the voids.

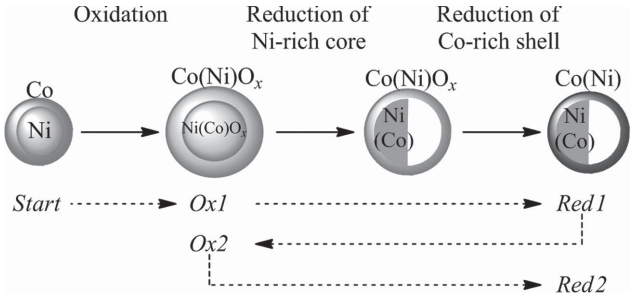

Scheme 1. Proposed mechanism for the morphology changes and nickel surface enrichment upon successive oxidations and reductions.

2.4. Surface Chemical State under Reaction Conditions

In this section we turn our attention to the state of the *NiCo* NPs in the presence of reaction mixtures of CO_2 and H_2, albeit at gas pressures (200 mTorr) substantially lower than those in Fischer-Tropsch type reactors. In the mTorr pressure range a very high coverage of adsorbates is still produced which, as previous experiments showed, can induce important changes in the NP structure.[18,41–46]

After introduction of CO_2 and H_2 the samples were heated to 250 °C while XPS were acquired (**Figure 4**). The Ni and Co 2p spectra were collected using a photon energy of 1115 eV and the 3p spectra with a photon energy of 700 eV. X-ray absorption spectra were also collected in the partial electron yield mode using the XPS analyzer with a kinetic energy of 580 eV for Co L-edge and 700 eV for Ni L-edge.

Upon heating to 200 °C under H_2 and CO_2, both nickel and cobalt were partially restored to the metallic state, as shown by the increase in the 2p peaks at 853.4 and 778.8 eV of Ni and Co, and the 3p peaks at 66.2 and 59.1 eV of Ni and Co, respectively (Figure 4a,b). This was accompanied by a corresponding decrease of the oxide peaks at ≈856 and 67 eV for Ni 2p and 3p, and 780 and 60 eV for Co 2p and 3p. Accordingly, the Ni L-edge (Figure 4c) and the Co L-edge (Figure S7, Supporting Information) spectra, with intense peaks at, respectively, 852.7 and 778 eV, are each characteristic of the metallic states. Both the XPS and XAS indicate that cobalt was still slightly oxidized, even at 250 °C, as shown by the contributions in the 780–783 eV in the XPS and 776.5, 779.1, and 781.0 eV in the XAS.

From the Ni3p and Co3p regions in Figure 4b, we can conclude that the relative ratio of these metals on the surface did not change upon heating under the reaction mixture of CO_2 and H_2.

In summary, in situ XPS and XAS experiments, albeit at lower pressure, confirm that the active catalytic surface contains a nickel–cobalt alloy together with phosphorus. This is discussed next.

2.5. Surface Phosphorus Species

Phosphorus from the partial decomposition of the tri-n-octylphosphine (TOP) ligands used in the first synthesis step,[47,48] was found to be present in the NPs (**Scheme 2**). Phosphorus can decrease the catalyst activity by blocking surface sites,[21] while at the same time increasing the selectivity for catalytic processes such as partial-hydrogenation of alkynes.[49–51] For that reason the amount and the nature of surface phosphorus species after oxidation, reduction, and under the reactant gases was monitored by XPS (**Figure 5**).

© 2015 Wiley-VCH Verlag GmbH & Co. KGaA, Weinheim

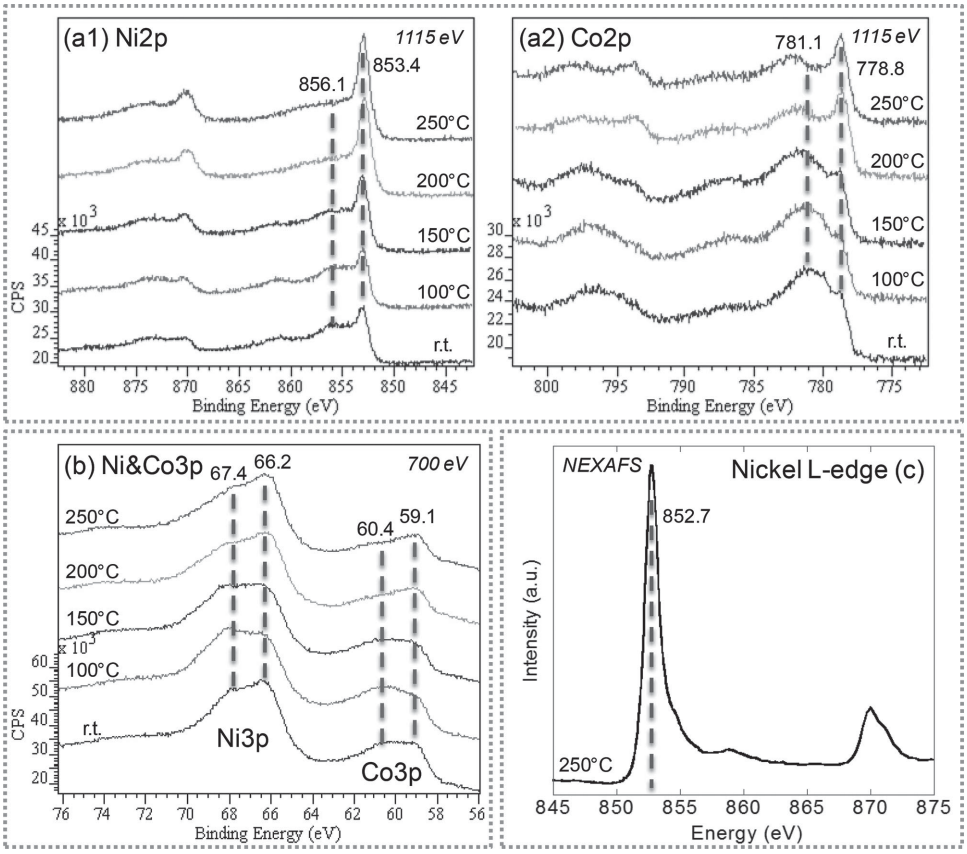

Figure 4. a) and b) APXPS of *NiCo* NPs exposed to a mixture of CO_2 and H_2 (100 mTorr each) as a function of temperature. c) NEXAFS of Ni L-edge at 250 °C under the mixture of CO_2 and H_2.

Phosphorus is known to be fairly mobile within metal NPs,[52–56] and was indeed detected by EDS, as shown in the Figure S2, Supporting Information. The total amount was estimated to be 10 mol% of the composition of the NPs. Two phosphorus-containing species were initially present in the nickel core (phosphide species, Scheme 2, blue dots)[47,48] and on the surface. The surface species is phosphine oxide from the oxidation of residual TOP ligands during transfer of the NPs in air (Scheme 2, black dots).

Initially only phosphine oxide was detected on the surface, as shown by the $2p_{3/2}$ and $2p_{1/2}$ doublet peak at 133.1 and 134.1 eV (Figure 5a, *Start*), which originated from the oxidation of TOP into trioctylphosphine oxide (TOPO) when exposed to air after synthesis and washing. The estimated surface fraction of phosphorus, using a mean free path value of 1.1 nm (700 eV photon energy), is ≈7% mol (Figure 5b, *Start*).

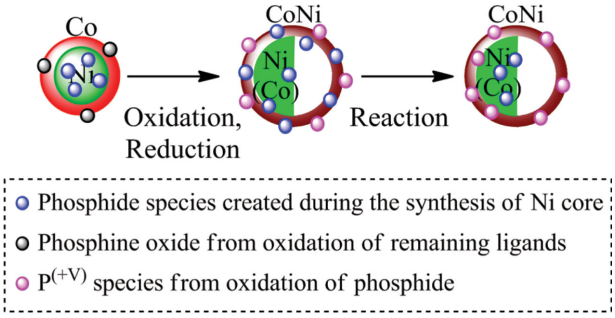

Scheme 2. Phosphorus species in *NiCo* NPs. Phosphides are more reduced species with B.E. in the 129 eV region. Phosphine oxides, with B.E. at ≈133 eV, are present initially and removed during the cycles of oxidation and reduction. $P^{(+V)}$ includes phosphate and hydrogen phosphate, with B.E. in the 133–135 eV region.

After the second reduction step (Figure 5, *Red2*), the overall surface phosphorus content increased to ≈17%. Phosphides were clearly observed by a new P 2p doublet peak at 129.4 eV, as a result of partial migration of P atoms from the Ni core to the outer regions of the NP (Scheme 2). STEM-EDS shows the presence and distribution of phosphorus and suggests that the core of the NPs still contained a significant proportion of the phosphide species (Figure 5c). On the surface, more oxidized species were also observed with a P $2p_{3/2}$ peak at 133.2 eV. Since the area of the 133.2 eV peak is larger than that of the initial TOPO species it is likely that these phosphorus species represent surface phosphates generated from the oxidation of surface phosphide upon exposing the NPs to O_2 (Scheme 2).

Under reaction conditions (Figure 5, *Reaction*) some surface phosphorus was lost, either by forming volatile species or by migrating back into the core, but its relative surface ratio (≈11%) was still higher than at the beginning. The phosphorus remaining at the surface produced a peak at 133.7 eV B.E., 0.5 eV higher than after reduction. This may indicate the formation of a new compound on the surface, such as hydrogenated $O{=}P(OH)(OR)_2$ species, in addition to phosphates (Figure 5a, *Reaction* and Scheme 2).

© 2015 Wiley-VCH Verlag GmbH & Co. KGaA, Weinheim

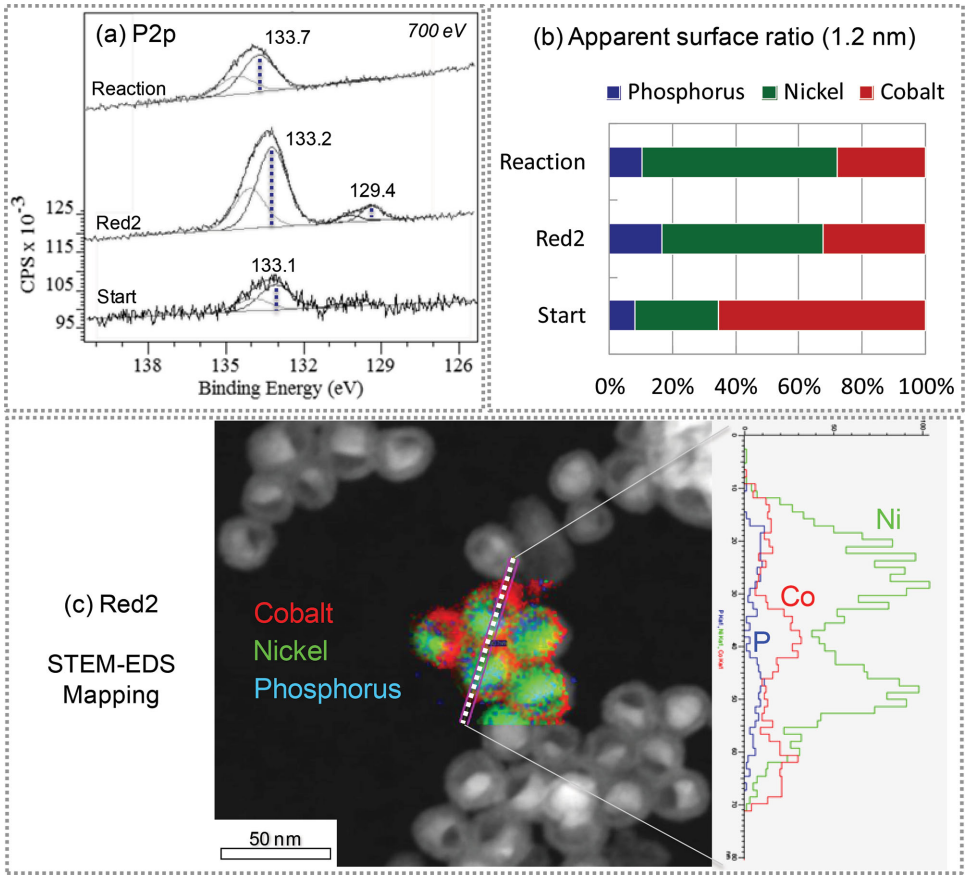

Figure 5. a) XPS from phosphorus species present in the *NiCo* NPs. After synthesis a doublet peak at 133.1 eV is observed corresponding to phosphine oxide (bottom curve, *Start*). After oxidation and reduction (*Red2*), a P peak from phosphide species appears at 129.4 eV due to segregation from the Ni core, most undergoing oxidation to give phosphate (133.2 eV). Under catalytic conditions (*Reaction*) some of the phosphate species undergo further transformation, likely to hydrogenated phosphate. b) Relative surface ratio of P, Ni, and Co calculated from the XPS peak intensities. c) Color-coded STEM map after reduction (*Red2)* and line profile over two NPs.

2.6. Catalytic Activity Measurements

To assess the ability of these NPs to convert CO_2 into useful products, we investigated their catalytic activity by depositing the NPs on a mesoporous silica support (MCF-17) with a loading of ≈5% metal by weight. Before the reaction with CO_2, the surfactants were removed by first heating in O_2 at 150 Torr for 1 h at 350 °C in a fixed bed reactor, followed by reduction with 150 Torr of H_2 for 1 h at 350 °C. The NPs were then exposed to a CO_2:H_2:He = 6.6:20.7:14.7 gas mixture at a total pressure of 6 bar and at two reaction temperatures, 200 and 350 °C.

We found that at 200 °C the CO_2 conversion was 0.24% and at 350 °C it increased to 0.92%. At 350 °C, the mass activity of the NiCo/P catalyst was ≈25 and ≈90 times lower than that of pure Co catalyst, calculated with and without CO as product, respectively. This is likely the result of blocking effects of P species on the surface. However, the *NiCo*/P catalyst presented an unexpected selectivity, producing oxygenates (methanol and formaldehyde) instead of methane and heavier alkanes, as would have been expected from nickel[22] or cobalt NPs.[21] As shown on **Figure 6**, *NiCo/P* catalyst exhibited a high selectivity for CO (between 75% and 85%), but they produced over 30% of formaldehyde at 200 °C and 10% of methanol at 350 °C.

These results suggest that *NiCo* NPs may be interesting catalysts for producing oxygenates from cheap carbon sources such as CO_2. Further investigations are underway to determine the influence of the NPs structure (morphology, surface alloy, and presence of phosphorus species) on the selectivity.

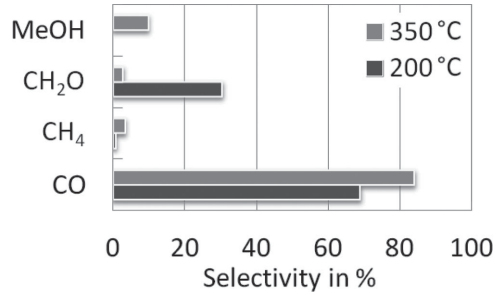

Figure 6. Selectivity of *NiCo* NPs for the reduction of CO_2 by H_2 at two different temperatures. Interestingly, the *NiCo* NPs produced oxygenates (CH_2O, MeOH) in addition to carbon monoxyde and almost no methane.

© 2015 Wiley-VCH Verlag GmbH & Co. KGaA, Weinheim

3. Conclusion

We have developed a new route for the synthesis of nickel–cobalt core–shell NP catalysts whose diameter and shell thickness can be tailored. We have shown that oxidation and reduction treatments to remove contaminants and ligands reduced the NPs to the metallic state, with profound effects on the morphology and surface composition. Reduction produced a peculiar core–shell structure, with a crystalline metallic core rich in Ni filling about half of the core and separated from the void by low Miller index planes. The shell consisted of a NiCo alloy in a ≈1:1 Ni:Co ratio, oxidized upon air exposure but metallic under the reducing environment of CO_2 and H_2 mixture. We also found that phosphorus, from the TOP ligands, was incorporated in the NPs and segregated to the surface during reaction to produce oxidized $P^{(+V)}$ species, likely phosphate. Our study shows the very large structural modifications that occur when the NPs are subjected to activation/cleaning treatments and under mixtures of CO_2 and H_2 reactants, demonstrating that the final structure of the operating catalysts can be very different from the original one, and is determined by the reactants surrounding them in equilibrium.

4. Experimental Section

(i) The *NiCo* NPs were prepared as follow in a two-step, one-pot procedure. The reactions were carried out under nitrogen atmosphere using standard Schlenk techniques.

Nickel Core: Nickel cores were synthesized from a reported procedure.[57] Briefly, $Ni(acac)_2$ (770 mg, 3.0 mmol) was added to 36.0 mmol of oleylamine (11.8 mL, 12 equivalents, Oleylamine 70% was purchased from Aldrich) and 9 mmol of TOP (4.0 mL, 3 equivalents, TOP 97% was purchased from Strem). The mixture was degassed at 100 °C, and heated at 220 °C for 2 h under inert atmosphere, giving quickly a black solution. After 2 h, the heating was stopped and the solution left to cool down to room temperature. The Ni(0) NPs solution was used as such for the second step after cooling down to room temperature (although a small aliquot was taken out for analysis).

Cobalt Shell: To the previous colloidal solution of nickel cores, 1.5 mmol of $Co_2(CO)_8$ (530 mg, 0.5 equivalents, purchased from Alpha-Aesar) was added. The solution was heated to 120 °C for 10 min, then the temperature was increased to 180 °C for 1 h. The solution was cooled down to room temperature and the NPs were collected with a magnet. They were washed four time by redispersion in hexanes (5 mL) and addition of 50 mL of isopropanol. The NPs were dried under a flow of N_2 and stored under N_2.

(ii) The chemical state of the surface of the NPs was analyzed in situ by APXPS, which allows exposure of the NPs to gases at pressures in the Torr range. The experiments were conducted at beamline 11.0.2 of the Advanced Light Source in Berkeley, California.[32] *NiCo* NPs were dissolved in hexanes using ultrasound warm bath (50 °C) and deposited on a warm gold foil (50 °C) by drop-casting of two drops of solution. Au4f and Au4d peaks were used to calibrate the binding energies of other peaks and to normalize the spectra, when required. The incident photon energy was 700 eV unless said otherwise. X-ray absorption spectra were recorded right before or after the APXPS measurements using the XPS analyzer as partial electron yield detector.

(iii) TEM grids were prepared by evaporating a drop of hexanes suspension of the NPs on a Si_3N_4 membrane (Ted Pella, INC). When required, the membranes were treated under O_2 or H_2 in a home-made U-shape quartz reactor, as described before.[18] They were treated under conditions similar to those in the APXPS experiments (oxidation at 220 °C and reduction at 270 °C) but at a total pressure of 1 bar. After treatment, the grid was taken out and transferred to the TEM in air and at room temperature. Analysis of the NPs was done using a JEOL 2100F TEM operated at 200 kV either in HRTEM mode, or in STEM mode with a probe size of 1 nm for HAADF and EDS-mapping analysis. It should be noted that the NPs were exposed to air at room temperature during the transfer of the grid from the reactor to the TEM.

(iv) Supported catalysts were prepared by impregnation of *NiCo* NPs on a silica support (MCF-17) in chloroform, washing three times in ethanol and drying overnight at 100 °C. A loading of 5% metal in weight was used. Catalytic studies were performed using the setup described.[21] Briefly, the catalyst sample (50 mg) was inserted in a steel tubular plug flow reactor (i.d. 3 mm) and retained between plugs of quartz wool, and the reactor temperature monitored with a K-thermocouple. A reactant gas feed consisting of CO_2 (BOC 99.5%), H_2 (Praxair 99.999%) balanced with He (Praxair 99.999%), in molar ratio CO_2:H_2:He = 6.6:20.7:14.7 was delivered via a series of independent calibrated mass flow controllers (MKS Instruments). The total flow was 42 sccm, giving a gas hourly space velocity of ≈60 000 h^{-1}. The pressure was regulated via a needle valve to 6 bar. The output gases were analyzed using a Hewlett Packard HP 5890 Series II chromatograph equipped with both FID and TCD detectors. Under these conditions CO_2 conversions were typically less than 10% to minimize the contribution of subsequent reactions of the primary products with the catalyst.

Supporting Information

Supporting Information is available from the Wiley Online Library or from the author.

Acknowledgements

Prof. A. P. Alivisatos, Brandon Beberwyck, and Matt Lucas are gratefully acknowledged for access to their NPs synthesis facility. This work was supported by the Director, Office of Science, Office of Basic Energy Sciences, Chemical Sciences, Geosciences, and Biosciences Division, under the Department of Energy Contract No. DE-AC02-05CH11231. The Molecular Foundry, a DOE Office of Science User facility, is acknowledged under Proposal No. 1510.

[1] K. Huang, C.-L. Sun, Z.-J. Shi, *Chem. Soc. Rev.* **2011**, *40*, 2435.
[2] C. Costentin, M. Robert, J.-M. Savéant, *Chem. Soc. Rev.* **2013**, *42*, 2423.

© 2015 Wiley-VCH Verlag GmbH & Co. KGaA, Weinheim

[3] A. Bachmeier, V. C. C. Wang, T. W. Woolerton, S. Bell, J. C. Fontecilla-Camps, M. Can, S. W. Ragsdale, Y. S. Chaudhary, F. A. Armstrong, *J. Am. Chem. Soc.* **2013**, *135*, 15026.
[4] X. Chen, Y. Zhou, Q. Liu, Z. Li, J. Liu, Z. Zou, *ACS Appl. Mater. Interfaces* **2012**, DOI 10.1021/am300661s.
[5] M. E. Dry, *Catal. Today* **2002**, *71*, 227.
[6] U. Rodemerck, M. Hole a, E. Wagner, Q. Smejkal, A. Barkschat, M. Baerns, *Chem Cat Chem* **2013**, *5*, 1948.
[7] Q. Zhang, J. Kang, Y. Wang, *Chem Cat Chem* **2010**, *2*, 1030.
[8] X.-Y. Quek, Y. Guan, R. A. van Santen, E. J. M. Hensen, *Chem Cat Chem* **2011**, *3*, 1735.
[9] R. A. van Santen, A. J. Markvoort, *Chem Cat Chem* **2013**, *5*, 3384.
[10] B. H. Davis, *Fuel Process. Technol.* **2001**, *71*, 157.
[11] S. Shetty, A. P. J. Jansen, R. A. van Santen, *J. Am. Chem. Soc.* **2009**, *131*, 12874.
[12] M. Ojeda, R. Nabar, A. U. Nilekar, A. Ishikawa, M. Mavrikakis, E. Iglesia, *J. Catal.* **2010**, *272*, 287.
[13] A. Tuxen, S. Carenco, M. Chintapalli, C.-H. Chuang, C. Escudero, E. Pach, P. Jiang, F. Borondics, B. J. Beberwyck, A. P. Alivisatos, G. Thornton, W.-F. Pong, J. Guo, R. Perez, F. Besenbacher, M. Salmeron, *J. Am. Chem. Soc.* **2013**, *135*, 2273.
[14] J. Schweicher, A. Bundhoo, A. Frennet, N. Kruse, H. Daly, F. C. Meunier, *J. Phys. Chem. C* **2010**, *114*, 2248.
[15] M. K. Gnanamani, M. C. Ribeiro, W. Ma, W. D. Shafer, G. Jacobs, U. M. Graham, B. H. Davis, *Appl. Catal. A* **2011**, *393*, 17.
[16] N. D. Subramanian, C. S. S. R. Kumar, K. Watanabe, P. Fischer, R. Tanaka, J. J. Spivey, *Catal. Sci. Technol.* **2012**, *2*, 621.
[17] S. K. Beaumont, S. Alayoglu, V. V. Pushkarev, Z. Liu, N. Kruse, G. A. Somorjai, *Faraday Discuss.* **2013**, *162*, 31.
[18] S. Carenco, A. Tuxen, M. Chintapalli, E. Pach, C. Escudero, T. D. Ewers, P. Jiang, F. Borondics, G. Thornton, A. P. Alivisatos, H. Bluhm, J. Guo, M. Salmeron, *J. Phys. Chem. C* **2013**, *117*, 6259.
[19] N. Kumar, M. L. Smith, J. J. Spivey, *J. Catal.* **2012**, *289*, 218.
[20] H. Wang, W. Zhou, J.-X. Liu, R. Si, G. Sun, M.-Q. Zhong, H.-Y. Su, H.-B. Zhao, J. A. Rodriguez, S. J. Pennycook, J.-C. Idrobo, W.-X. Li, Y. Kou, D. Ma, *J. Am. Chem. Soc.* **2013**, *135*, 4149.
[21] V. Iablokov, S. K. Beaumont, S. Alayoglu, V. V Pushkarev, C. Specht, J. Gao, A. P. Alivisatos, N. Kruse, G. A. Somorjai, *Nano Lett.* **2012**, *12*, 3091.
[22] V. Sanchez-Escribano, M. A. Larrubia Vargas, E. Finocchio, G. Busca, *Appl. Catal. A* **2007**, *316*, 68.
[23] Y. Yu, G. Jin, Y. Wang, X. Guo, *Catal. Commun.* **2013**, *31*, 5.
[24] M. Mihaylov, K. Hadjiivanov, H. Knözinger, *Catal. Lett.* **2001**, *76*, 59.
[25] S. Carenco, C. Boissière, L. Nicole, C. Sanchez, P. Le Floch, N. Mézailles, *Chem. Mater.* **2010**, *22*, 1340.
[26] S. Carenco, S. Labouille, S. Bouchonnet, C. Boissière, X.-F. Le Goff, C. Sanchez, N. Mézailles, *Chem. Eur. J.* **2012**, *18*, 14165.
[27] T. Yamauchi, Y. Tsukahara, K. Yamada, T. Sakata, Y. Wada, *Chem. Mater.* **2011**, *23*, 75.
[28] G. F. Pregaglia, A. Andreetta, G. F. Ferrari, G. Montrasi, R. Ugo, *J. Organomet. Chem.* **1971**, *33*, 73.
[29] J. V. I. Timonen, E. T. Seppälä, O. Ikkala, R. H. a Ras, *Angew. Chem. Int. Ed. Engl.* **2011**, *50*, 2080.
[30] V. F. Puntes, K. M. Krishnan, A. P. Alivisatos, *Science* **2001**, *291*, 2115.
[31] J. V. I. Timonen, E. T. Seppälä, O. Ikkala, R. H. A. Ras, *Angew. Chem. Int. Ed. Engl.* **2011**, *50*, 2080.
[32] D. Frank Ogletree, H. Bluhm, E. D. Hebenstreit, M. Salmeron, *Nucl. Instrum. Methods Phys. Res. Sect. A.* **2009**, *601*, 151.
[33] H. Bluhm, M. Hävecker, A. Knop-Gericke, M. Kiskinova, R. Schlögl, M. Salmeron, *MRS Bull.* **2011**, *32*, 1022.
[34] D. E. Starr, Z. Liu, M. Hävecker, A. Knop-Gericke, H. Bluhm, *Chem. Soc. Rev.* **2013**, *42*, 5833.
[35] J. J. Yeh, I. Lindau, *At. Data Nucl. Data Tables* **1985**, *32*, 1.
[36] C. J. Powell, A. Jablonski, *NIST Electron Inelastic-Mean-Free-Path Database, Version 1.2*, National Institute of Standards and Technology, Gaithersburg, MD **2010**.
[37] M. P. Seah, *Surf. Interface Anal.* **2012**, *44*, 497.
[38] M. L. Smith, A. Campos, J. J. Spivey, *Catal. Today* **2012**, *182*, 60.
[39] T. Osawa, T. Kizawa, I.-Y. S. Lee, S. Ikeda, T. Kitamura, Y. Inoue, V. Borovkov, *Catal. Commun.* **2011**, *15*, 15.
[40] J. G. Railsback, A. C. Johnston-Peck, J. Wang, J. B. Tracy, *ACS Nano* **2010**, *4*, 1913.
[41] M. Salmeron, R. Schlogl, *Surf. Sci. Rep.* **2008**, *63*, 169.
[42] M. Hävecker, R. W. Mayer, A. Knop-Gericke, H. Bluhm, E. Kleimenov, A. Liskowski, D. Su, R. Follath, F. G. Requejo, D. F. Ogletree, M. Salmeron, J. A. Lopez-Sanchez, J. K. Bartley, G. J. Hutchings, R. Schlögl, *J. Phys. Chem. B* **2003**, *107*, 4587.
[43] B. Halevi, E. J. Peterson, A. DeLaRiva, E. Jeroro, V. M. Lebarbier, Y. Wang, J. M. Vohs, B. Kiefer, E. Kunkes, M. Havecker, M. Behrens, R. Schlögl, A. K. Datye, *J. Phys. Chem. C* **2010**, *114*, 17181.
[44] B. Halevi, E. J. Peterson, A. Roy, A. DeLariva, E. Jeroro, F. Gao, Y. Wang, J. M. Vohs, B. Kiefer, E. Kunkes, M. Hävecker, M. Behrens, R. Schlögl, A. K. Datye, *J. Catal.* **2012**, *291*, 44.
[45] S. Piccinin, S. Zafeiratos, C. Stampfl, T. W. Hansen, M. Hävecker, D. Teschner, V. I. Bukhtiyarov, F. Girgsdies, A. Knop-Gericke, R. Schlögl, M. Scheffler, *Phys. Rev. Lett.* **2010**, *104*, 035503.
[46] R. Arrigo, M. Hävecker, M. E. Schuster, C. Ranjan, E. Stotz, A. Knop-Gericke, R. Schlögl, *Angew. Chem. Int. Ed. Engl.* **2013**, *52*, 11660.
[47] L. M. Moreau, D.-H. Ha, C. R. Bealing, H. Zhang, R. G. Hennig, R. D. Robinson, *Nano Lett.* **2012**, *12*, 4530.
[48] L. M. Moreau, D. Ha, H. Zhang, R. Hovden, D. A. Muller, R. D. Robinson, *Chem. Mater.* **2013**, *25*, 2394.
[49] X. Li, Y. Zhang, A. Wang, Y. Wang, Y. Hu, *Catal. Commun.* **2010**, *11*, 1129.
[50] H. Wang, Y. Shu, M. Zheng, T. Zhang, *Catal. Lett.* **2008**, *124*, 219.
[51] S. Carenco, A. Leyva-Pérez, P. Concepción, C. Boissière, N. Mézailles, C. Sanchez, A. Corma, *Nano Today* **2012**, *7*, 21.
[52] L. De Trizio, A. Figuerola, L. Manna, A. Genovese, C. George, R. Brescia, Z. Saghi, R. Simonutti, M. Van Huis, A. Falqui, *ACS Nano* **2012**, *6*, 32.
[53] D.-H. Ha, L. M. Moreau, C. R. Bealing, H. Zhang, R. G. Hennig, R. D. Robinson, *J. Mater. Chem.* **2011**, *21*, 11498.
[54] S. Carenco, Y. Hu, I. Florea, O. Ersen, C. Boissière, C. Sanchez, N. Mézailles, *Dalton Trans.* **2013**, *42*, 12667.
[55] S. Carenco, Y. Hu, I. Florea, O. Ersen, C. Boissière, N. Mézailles, C. Sanchez, *Chem. Mater.* **2012**, *24*, 4134.
[56] S. Carenco, X. F. Le Goff, J. Shi, L. Roiban, O. Ersen, C. Boissière, C. Sanchez, N. Mézailles, *Chem. Mater.* **2011**, *23*, 2270.
[57] S. Carenco, C. Boissière, L. Nicole, C. Sanchez, P. Le Floch, N. Mézailles, C. Boissiere, N. Mezailles, *Chem. Mater.* **2010**, *22*, 1340.

Received: September 16, 2014
Revised: November 18, 2014
Published online: February 26, 2015

© 2015 Wiley-VCH Verlag GmbH & Co. KGaA, Weinheim